[논 문] 한국재료학회지
Korean J. Mater. Res.
Vol. 26, No. 8 (2016)

http://dx.doi.org/10.3740/MRSK.2016.26.8.430

Atomic Layer Deposition of Al_2O_3 Thin Films Using Dimethyl Aluminum *sec*-Butoxide and H_2O Molecules

Byeonghyeon Jang and Soo-Hyun Kim†

School of Materials Science and Engineering, Yeungnam University, Gyeongsan-si 38541, Republic of Korea

(Received June 22, 2016 : Revised June 22, 2016 : Accepted July 8, 2016)

Abstract Aluminum oxide (Al_2O_3) thin films were grown by atomic layer deposition (ALD) using a new Al metalorganic precursor, dimethyl aluminum *sec*-butoxide ($C_{12}H_{30}Al_2O_2$), and water vapor (H_2O) as the reactant at deposition temperatures ranging from 150 to 300 °C. The ALD process showed typical self-limited film growth with precursor and reactant pulsing time at 250 °C; the growth rate was 0.095 nm/cycle, with no incubation cycle. This is relatively lower and more controllable than the growth rate in the typical ALD-Al_2O_3 process, which uses trimethyl aluminum (TMA) and shows a growth rate of 0.11 nm/cycle. The as-deposited ALD-Al_2O_3 film was amorphous; X-ray diffraction and transmission electron microscopy confirmed that its amorphous state was maintained even after annealing at 1000 °C. The refractive index of the ALD-Al_2O_3 films ranged from 1.45 to 1.67; these values were dependent on the deposition temperature. X-ray photoelectron spectroscopy showed that the ALD-Al_2O_3 films deposited at 250 °C were stoichiometric, with no carbon impurity. The step coverage of the ALD-Al_2O_3 film was perfect, at approximately 100 %, at the dual trench structure, with an aspect ratio of approximately 6.3 (top opening size of 40 nm). With capacitance-voltage measurements of the Al/ALD-Al_2O_3/p-Si structure, the dielectric constant of the ALD-Al_2O_3 films deposited at 250 °C was determined to be ~8.1, with a leakage current density on the order of 10^{-8} A/cm^2 at 1 V.

Key words aluminium oxide, atomic layer deposition, dimethyl aluminum *sec*-butoxide, trimethyl aluminum, growth rate.

1. Introduction

With the continuous scaling down of Si-based semiconductor devices, many materials have been identified as high-permittivity(high-*k*) materials with a higher dielectric constant than SiO_2 for their better performance and greater functionality.[1-2] Important concerns on them include the interface quality,[2-3] film morphology,[4-5] and reliability. Among them, aluminum oxide (Al_2O_3) thin films[3,6-10] have been studied extensively and applied to commercial logic devices[11] and dynamic random access memory(DRAM)[12] as a gate oxide or capacitor dielectric owing to its excellent properties, such as high band gap (8~9 eV) leading to a low leakage current, high thermal stability to maintain an amorphous structure up to 1000 °C annealing, good interface with Si, resulting in a low defect density ($< 10^{11}$ cm^{-2}), and a high negative fixed charge density ($> 10^{12}$ cm^{-2}).[13-15] Apart from its main applications for semiconductor devices mentioned above, Al_2O_3 thin films are commonly used as a protective layer and ion barrier for photovoltaic cells and gas diffusion barriers for organic displays.[16-18] All these applications require the Al_2O_3 films to have good homogeneity, low surface roughness, and good control of the film thickness for films in the order of 10 Å or less. A range of deposition techniques, such as sputtering,[19] chemical vapor deposition,[15,20] pulsed laser deposition,[21] and thermal evaporation[22] have been introduced for preparing the Al_2O_3 thin films. On the other hand, these methods have an inherent limitation to be applied for potential higher performance devices with very complex, small sized, and high aspect ratio structures. Atomic layer deposition (ALD) can provide a viable solution for the deposition of Al_2O_3 thin films for those emerging applications because ALD can provide excellent conformality, digital controllability of the film thickness, and large-area uniformity owing to its inherent surface-saturated and self-limited reaction mechanisms.[23]

Many Al precursors have been identified for successful ALD-Al_2O_3 processes[24-29] but alkyl aluminum or alkyl

†Corresponding author
E-Mail : soohyun@ynu.ac.kr (S.-H. Kim, Yeungnam Univ.)

aluminum hydride is typically used for commercial ALD-Al_2O_3 processes[30-33] because they have high vapor pressures [e.g., in the case of trimethyl aluminum(TMA), 9 torr at 20 °C] to guarantee a reliable supply of the precursor into the deposition chamber, relatively inexpensive, very reactive with typical oxidants, such as H_2O, O_2, and O_3, and relatively low temperature growth is possible. In the growth process using a liquid source of TMA and H_2O, it is unnecessary to recharge the source materials for every run, which is in contrast to the process using solid source, such as $AlCl_3$. One of the disadvantages of alkyl aluminum precursors, such as TMA is that they are pyrophoric, which requires special handling and storage precautions.[8] In addition, ultra-thin thickness control is difficult in the ALD-Al_2O_3 process using TMA because of the relatively rapid growth rate.[34] In addition, the TMA precursor in ALD has a disadvantage of the incorporation of impurities, C and H, during film growth via a reaction between the precursor and reactant. Incorporated H was reported to increase the leakage current of the dielectric layer[35] and the as-deposited Al_2O_3 films showed a very large leakage current compared to those of post-annealed films.[36] To address these problems with ALD-Al_2O_3 processes, other Al metalorganic precursors, such as aluminum isopropoxide ($C_9H_{21}AlO_3$), have been used. On the other hand, this compound polymerizes easily and exists as a mixture of polymers or oligomers.[37] Each polymer or oligomer has a different vapor pressure. As a result, the vapor pressure of this precursor is unpredictable and difficult to control. Aluminum 2-ethylhexanoate ($C_{16}H_{31}AlO_5$) has also been used as a precursor for the ALD-Al_2O_3 process, but its low vapor pressure results in a low deposition rate, which limits its use.

In this study, Al_2O_3 thin films were deposited by ALD using new non-pyrophoric Al precursor, dimethyl aluminum *sec*-butoxide (DMASBO, $C_{12}H_{30}Al_2O_2$), which is even stable in air and the vapor pressure is sufficiently high to be applied to ALD with H_2O as a reactant. The growth kinetics at deposition temperatures ranging from 150 to 300 °C was investigated and compared with that of the TMA-based ALD-Al_2O_3 process. In addition, film properties, such as the phase, density, refractive index, composition, step coverage, and thermal stability were characterized using a range of analysis tools. Finally, ALD-Al_2O_3 films were evaluted as a capacitor dielectric.

2. Experimental Procedure

Al_2O_3 thin films were deposited in a travelling-wave type ALD reactor (Lucida-D100, NCD technology) using a new Al metalorganic precursor, (dimethyl aluminum *sec*-butoxide) ($C_{12}H_{30}Al_2O_2$) and water vapor as the reactant. The new Al metalorganic precursor is liquid at room temperature and has a vapor pressure of 0.9 Torr at 63 °C. Fig. 1 shows the molecular structure of the Al precursor used in this study. The deposition temperatures ranging from 150 and 300 °C were varied to find a possible ALD temperature window of the present ALD scheme whereas the typical deposition temperature was 250 °C. P-type Si (100) wafers covered with 100-nm-thick thermally grown SiO_2 were used as the substrates. The chamber was evacuated to ~ 0.05 Torr prior to deposition and the chamber pressure was approximately 0.5 Torr during deposition. The precursor was heated to 56 °C to reliably provide the precursor to the chamber and the temperature of the precursor delivery line was maintained at 100 °C to prevent condensation of the Al precursor during delivery. Water vapor, which was carried by 100 sccm of N_2 gas, was also provided to the chamber as a reactant. Between the precursor and reactant pulsing steps, a purging process was performed with 200 sccm of N_2; each ALD cycle involved precursor pulsing, purging, reactant pulsing, and purging. From preliminary investigations, basic pulsing conditions were set as follows: precursor pulsing for 3 s, reactant pulsing for 1 s, and purging for 10 s. Such a condition was sufficient to guarantee self-limited growth of the ALD-Al_2O_3 films.

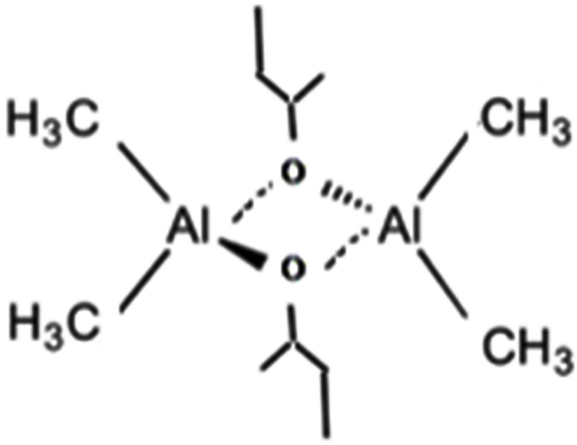

Fig. 1. The molecular structure of the Al precursor used in this study.

The thickness and density of the Al_2O_3 films were determined by X-ray reflectance (XRR, PANalytical X'-pert MRD with Cu-K_α radiation at 1.5 kW). For phase identification, grazing-incidence angle (incident angle, $\theta = 3^o$) X-ray diffraction (GIAXRD, PANalytical X'-pert MRD with Cu-K_α radiation at 1.5 kW) analysis was performed. The refractive indices of the films were measured by spectroscopic ellipsometry. The composition and chemical bonding within the Al_2O_3 films were analyzed by X-ray photoelectron spectroscopy (XPS, K-Alpha XPS Spectrometer with monochromated AI Ka in

Yeungnam University). Plan view transmission electron microscopy (Tecnai F20 equipped with 200 kV accelerating voltage and field emission gun) was used to examine the microstructures of the ALD-Al_2O_3 films. The step coverages of the films was evaluated on dual trench structures with an aspect ratio(AR) of ~6.3(bottom width: 15 nm) using cross-sectional view transmission electron microscopy(XTEM). The electrical properties, such as capacitance and leakage current of the fabricated MOS capacitor sample were measured using a probe station(Keithley 306 electrometer).

3. Results and Discussion

3.1 Growth kinetics of ALD-Al_2O_3 process

The growth kinetics of the ALD-Al_2O_3 process was examined at a deposition temperature of 250 °C. Fig. 2(a) shows the growth rates of the films as a function of the precursor pulsing time at a fixed reactant pulsing time of 1 s. The growth rates were determined by dividing the measured film thicknesses by the number of ALD reaction cycles. With increasing precursor pulsing time from 1 s to 3 s, the growth rate was increased; the grow rate was changed slightly by further increasing the precursor pulsing time to 5 s. The growth kinetics was also investigated according to the reactant pulsing time at a fixed precursor pulse time of 3 s(Fig. 2(b)). The results showed a constant growth rate at a very short pulse of H_2O longer than 0.5 s. These results clearly show that self-limited growth behavior of the ALD-Al_2O_3 films occurred using the new Al metalorganic precursor and H_2O. Fig. 2(c) shows the thicknesses of the ALD-Al_2O_3 films deposited using the basic pulsing conditions as a function of the number of ALD reaction cycles at 250 °C. For comparison, the results obtained using TMA and water vapor at the same deposition temperature are also shown. For both processes, the Al_2O_3 film thicknesses were increased linearly with increasing number of ALD reaction cycles, which is a typical characteristic of ALD process, and the extrapolated lines clearly showed that no incubation cycles were required for ALD-Al_2O_3 film growth. On the other hand, the growth rate of the DMASBO-based ALD-Al_2O_3 process was slightly lower (0.095 nm/cycle) than that of the TMA-based ALD-Al_2O_3 process (0.125 nn/cycle). Indeed, many reports on the ALD-Al_2O_3 process using TMA and H_2O vapor showed growth rates ranging from 0.1 nm/cycle to 0.13 nm/cycle,[5,9,24,38,39] which were higher than that from the present new Al precursor.

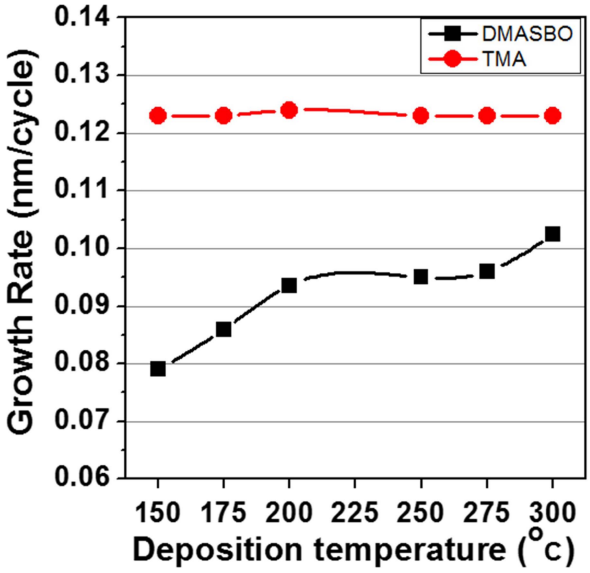

Fig. 3. Growth rates of the ALD-Al_2O_3 films as a function of the deposition temperature from 150 and 300 °C. The basic pulsing conditions that guaranteed self-limited film growth were used (precursor pulsing of 3 s, reactant pulsing of 1 s, and precursor and reactant purging of 10 s).

Fig. 3 shows the growth rates of both ALD-Al_2O_3 processes obtained under the basic pulsing condition as a function of the deposition temperature. The deposition

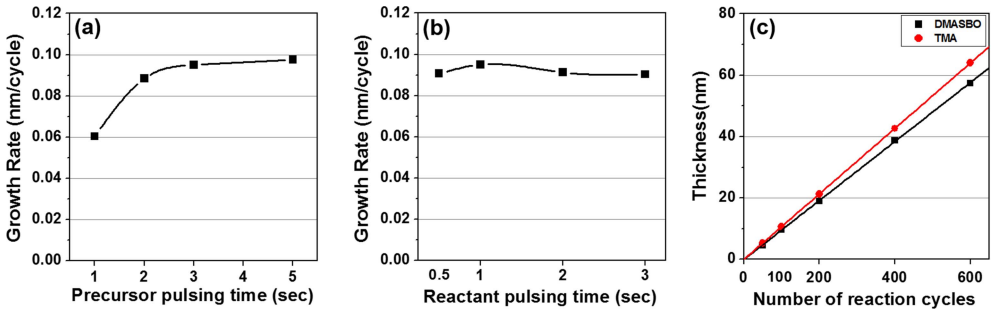

Fig. 2. Growth rate of ALD-Al_2O_3 films deposited on SiO_2 substrates after 200 cycles as a function of (a) the Al precursor pulsing time and (b) reactant (H_2O molecule) pulsing time. (c) Thickness of the ALD-Al_2O_3 films deposited on SiO_2 substrates as a function of the number of reaction cycles for different ALD-Al_2O_3 processes. The films were deposited at 250 °C under the basic pulsing conditions. The line indicates the linearly fitted line for the thickness data. The thicknesses were measured by X-ray reflectance (XRR) analysis.

temperature was varied from 150 to 300 °C. The growth rate of the TMA-based ALD-Al_2O_3 process was relatively constant, ~0.125 nm/cycle, irrespective of the deposition temperature. On the other hand, the growth rate of the DMASBO-based ALD-Al_2O_3 process was dependent on the deposition temperature and generally increased with increasing deposition temperature. At a deposition temperature of 150 °C, the growth rate of the DMASBO-based ALD-Al_2O_3 process was 0.078 nm/cycle, which is ~38 % lower than that of the TMA-based one. The growth rate was relatively constant, ~0.095 nm/cycle at deposition temperatures ranging from 200 and 275 °C, which is called the ALD temperature window. Above the ALD temperature window, the grow rate again increased to 0.102 nm/cycle but it was still lower than that of the TMA-based one. This indicates that the DMASBO-based ALD-Al_2O_3 process has greater potential than the TMA-based ALD-Al_2O_3 process in view of the process controllability, particularly for very thin films.

3.2 Properties of ALD-Al_2O_3 film

The ALD-Al_2O_3 films deposited under the basic conditions(at 250 °C within ALD temperature window) were analyzed using a range of techniques. Fig. 4 shows the refractive index and film density of the DMASBO-based ALD-Al_2O_3 films as a function of the deposition temperature from 150 to 300 °C, which were characterized by ellipsometry and X-ray reflectance analysis(XRR), respectively. The film density of the ALD-Al_2O_3 film increased from 2.77 to 3.14 g/cm^3 with increasing deposition temperature from 150° to 300 °C, which is a similar result to that of the TMA-based ALD-Al_2O_3 films.[9,14] For example, Oili et al. reported similar results in that the film density increased almost linearly with increasing ALD temperature from 2.85 to 3.10 g/cm^3 for the films grown at 110 to 300 °C.[40] The refractive index of the ALD-Al_2O_3 films also increased from 1.45 to 1.67 with increasing deposition temperature from 150 to 300 °C and showed a relatively constant value of ~1.6 for the films deposited within the ALD temperature window. The relationship between the film density and refractive

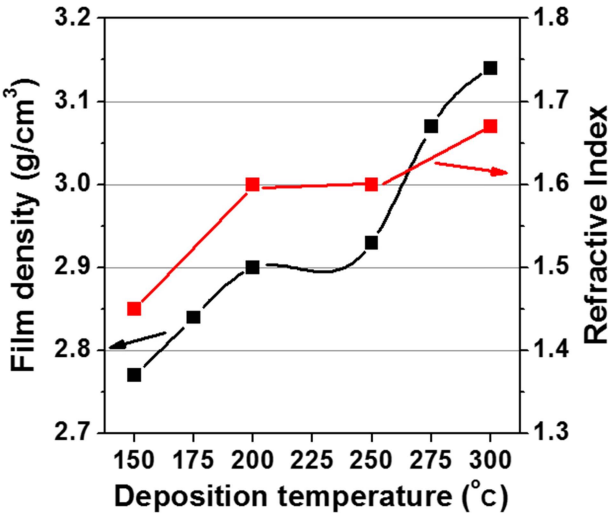

Fig. 4. Refractive index and film density as a function of the deposition temperature from 150 and 300 °C.

index can be calculated from the Gladstone-Dale equation (1) or the Lorentz-Lorenz equation (2), where ρ is the density, n is the refractive index, and K_1 and K_2 are constants. This means the refractive index is related to the film density, as shown in Fig. 3.[14,24]

$$\rho = K_1(n - 1) \quad \text{Eq. (1)}$$

$$\rho = K_2(n^2 - 1) / (n^2 + 2) \quad \text{Eq. (2)}$$

The films deposited under the basic pulsing conditions at 250 °C were analyzed further by XPS to identify the chemical bonding configurations. A survey spectrum acquired at the film surface in the binding energy range of 0~1204 eV(not shown here) showed signals of C(due to surface carbon contamination) as well as Al and O. Therefore, the XPS data were obtained after sputtering an approximately 4-nm-thick film to remove surface contamination and to characterize the bonding status of the film itself. As shown in Fig. 5(a), the C *1s* peak, which is generally shown at ~285 eV, was not detected, indicating that the film does not contain C. Fig. 5(b) showed

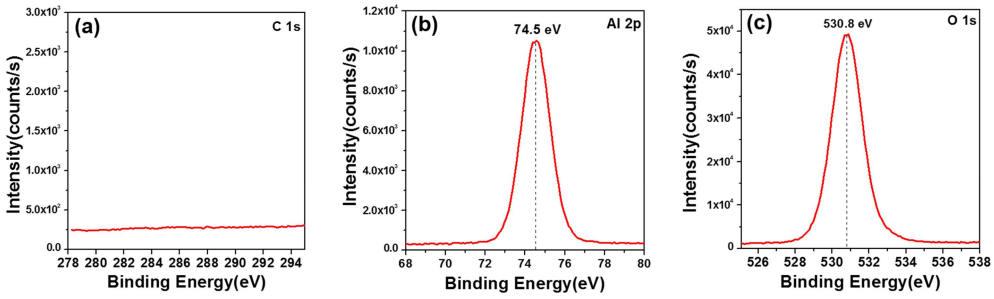

Fig. 5. XPS spectra of the ALD-Al_2O_3 film deposited at 250 °C with the basic pulsing conditions (3s-10s-1s-10s); (a) C 1*s* (b) Al 2*p*, (c) O 1*s* at after etching.

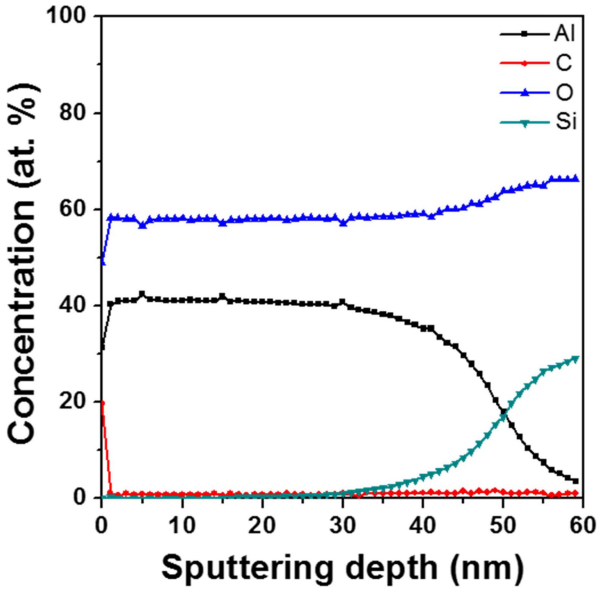

Fig. 6. XPS depth profile of ALD-Al_2O_3 films grown on SiO_2 substrates.

the binding energy of the Al *2p* photoelectron and the XPS data were calibrated to the adventitious C *1s* peak detected on the film surface. An intensive single peak at 74.5 eV was observed and attributed to Al-O bonding. The absence of a shoulder peak around 72.5 eV indicates that there were no Al-Al bonds in the film.[3,41] This is probably due to the completely oxidized aluminum by the self-limited surface reaction during the ALD process. In the case of the O *1s* XP spectrum, only a single peak centered at ~530.8 eV was observed, which was assigned to Al-O bonding in the Al_2O_3(Fig. 5(c)). Therefore, XPS analysis strongly supports that the films deposited using a new Al metalorganic precursor, DMASBO, consisted mostly of an Al_2O_3 phase.

Fig. 6 shows the XPS depth profile of the Al_2O_3 film deposited on a SiO_2 substrate. After sputtering an approximately 2-nm-thick film to remove surface contamination, the composition of each element was uniform throughout the film thickness. From the aforementioned result, incorporation of carbon impurity was negligible (less than 0.1 at.%) within the film, indicating that a high-purity Al_2O_3 film was deposited. The aluminum to oxygen ratio was quite stoichiometric, 2:3, corresponding to the Al_2O_3 composition. Therefore, this indicates that a very pure and quite stoichiometric ALD-Al_2O_3 film was deposited using the DMASBO precursor and H_2O as a reactant.

Fig. 7(a) shows the the grazing incident angle (incidence angle = 3º) XRD analysis result of the ALD-Al_2O_3 film deposited under the basic pulsing conditions at 250 °C. The grazing-angle XRD is more sensitive for characterizing the crystallinity and phase of ultrathin and nanocrystalline films. Even with sensitive grazing-angle XRD analysis, the result does not show any specific crystalline peaks related to crystalline Al_2O_3 and the intensive peak from single crystal Si was only observed at 56°. This suggests that the ALD-Al_2O_3 film forms an amorphous phase, which is similar to that in other deposition systems, such as sputtering, pulsed laser deposition, and chemical vapor deposition.[42-43] The results of the ALD-Al_2O_3 prepared using other Al metalorganic precursor also showed the formation of an as-deposited amorphous phase. The plan-view TEM image of the ALD-Al_2O_3(~20 nm-thick) (Fig. 7(b)) shows the microstructure of the film more obviously. This appears to be featureless, which is typical in an amorphous structure. The corresponding selected-area electron diffraction analysis [inset of Fig. 7(b)] showed a halo pattern and confirmed that the film was amorphous.

The thermal stability of the ALD-grown Al_2O_3 films was examined by annealing the films at high temperatures because one of the main applications of ALD-Al_2O_3 in this study is its use as a capacitor dielectric in DRAM devices. For example, during DRAM fabrication, the film may experience several high temperature processes after deposition and possible crystallization may often lead to a modification of the functional properties, such as an increase in leakage current in a DRAM capacitor. Fig. 7(c) shows the grazing incident angle XRD results of the films annealed at various temperatures. No remarkable changes in the XRD results were shown,

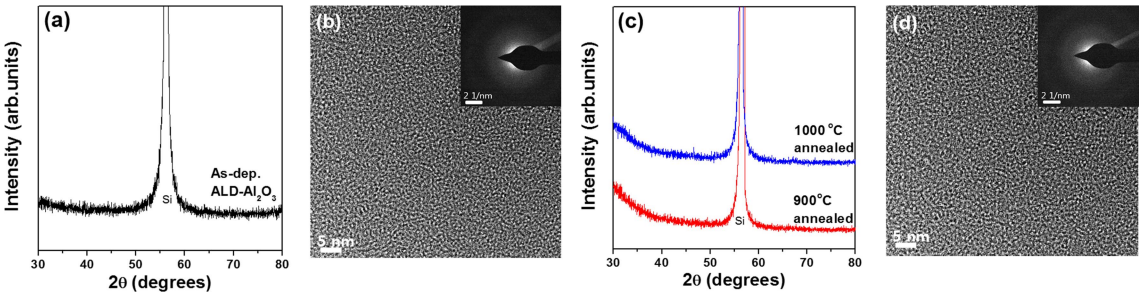

Fig. 7. (a) Grazing-angle XRD analysis results (b) plan-view TEM image of ALD-Al_2O_3 films deposited with basic pulsing condition at 250 °C. (c) grazing-angle XRD pattern (d) the plan view TEM image of ALD-Al_2O_3 film annealed at the annealing temperature.

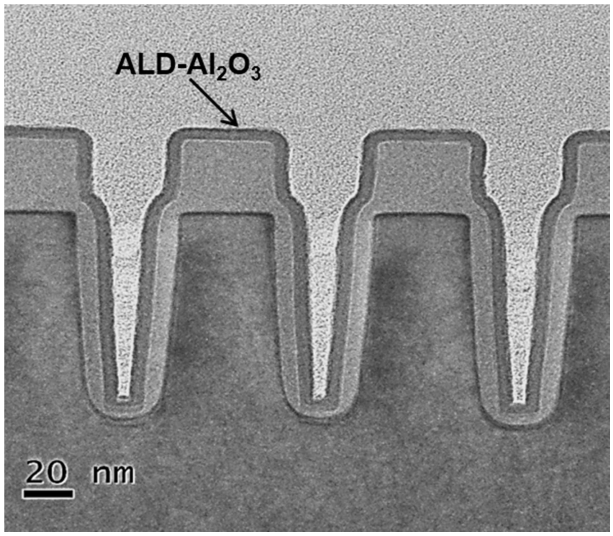

Fig. 8. Cross-section TEM image of the ALD-Al_2O_3 film deposited on the dual trench structures with a bottom width of ~15 nm and an AR of 6.3, showing the step coverage of the process.

even after annealing up to 1000 °C compared to that of the as-deposited film shown at Fig. 7(a). A plan-view TEM image of ALD-Al_2O_3 film annealed at 1000 °C(Fig. 7(d)) still appeared to be featureless, which is the same as that of as-deposited film shown at Fig. 7(b). The corresponding selected-area electron diffraction analysis [inset of Fig. 7(d)] showed a halo pattern and confirmed that the film is amorphous. Jakschik et al. reported that an ALD-Al_2O_3 film deposited using TMA and H_2O as a reactant remains amorphous up to 900 °C and crystallization proceeded at temperatures above 900 °C.[44] In addition, an ALD-Al_2O_3 film deposited using TMA and O_2 plasma as a reactant crystallized with a mass loss of ~5 % and a densification of ~20 % after annealing above 800 °C.[14] Therefore, the present results indicate that ALD-Al_2O_3 film developed in this study has better thermal stability than the ALD-Al_2O_3 film deposited using TMA.

The conformality of the new ALD-Al_2O_3 process was evaluated by depositing the film onto the overall nano-scale dual trench structure (top and bottom width: 40 and 15 nm, respectively) with an aspect ratio of ~6.3. The XTEM image(Fig. 8) clearly shows that the ALD-Al_2O_3 film was deposited conformally and uniformly on to the surface of the nano-scale dual trench indicating that the step coverage of the ALD-Al_2O_3 film was perfect at approximately 100 %. This perfect step coverage indicated that the Al_2O_3 film had been deposited under an ideal ALD growth process without partial decomposition of the DMASBO precursors.

Finally, to examine the electrical properties of the DMASBO-based ALD-Al_2O_3 films, the MOS capacitor structure sample (Al/Al_2O_3/p-Si) was fabricated with the Al_2O_3 film (32 nm in thickness) deposited at 250 °C. The capacitor area was 3.85×10^{-3} cm^2, which was defined by sputtering using a shadow mask during Al metal electrode (100 nm in thickness) deposition. Fig. 9(a) shows the capacitance-voltage results of the ALD-Al_2O_3 film using DMASBO, as measured at 100 KHz. The gate voltage was swept from the accumulation region (−5.0 V) to the inversion region (5.0 V) and back. This shows the typical features of a n-type metal oxide semiconductor (n-MOS) capacitor with an accumulation region at negative biases and an inversion region at positive biases. These small hysteresis loops are believed to be due to the low impurity content in the film.[41] The maximum accumulation capacitance of the ALD-Al_2O_3 using the DMASBO precursor was 810 pF at a gate bias of −5.0 V. The measured capacitance is similar to the serial capacitance of the grown ALD-Al_2O_3 and adventitious native SiO_2 layer. Considering the measured 2 nm thickness the

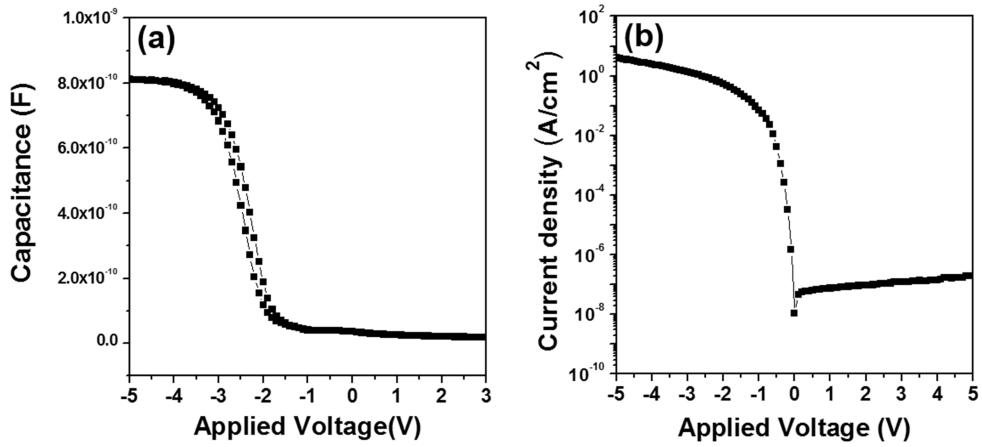

Fig. 9. (a) Capacitance-voltage characteristics of the Al_2O_3 film deposited at 250 °C from Al/ALD-Al_2O_3/p-Si capacitor. The data were recorded from accumulation to inversion, and back to accumulation. (b) Current density-voltage characteristics of the Al_2O_3 film deposited at 250 °C from an Al/ALD-Al_2O_3/p-Si capacitor.

native SiO_2 layer, the dielectric constant was calculated from the C-V data of Fig. 9(a). The estimated dielectric constant of the ALD-Al_2O_3 using the DMASBO precursor was 8.1. As expected, the dielectric constants of the ALD-Al_2O_3 film were lower than that of bulk α-Al_2O_3(~9), due to the lower density, as mentioned above. Fig. 9(b) shows the I-V characteristics of the ALD-Al_2O_3 film with the Al/ALD-Al_2O_3(32 nm in thickness)/p-Si capacitor structure. The leakage current density of the Al_2O_3 film using the DMASBO precursor was in the order of ~10^{-8} A/cm^2. The leakage current value was either similar to or slightly higher than that of the TMA-based ALD-Al_2O_3 studies and indicates that the DMASBO-based ALD-Al_2O_3 process is not inferior to the electrical properties, such as dielectric constant and leakage current, compared to that of the TMA-based ALD-Al_2O_3 process.[6-9)]

4. Summary and Conclusions

In this study, Al_2O_3 films were deposited on thermally grown SiO_2 substrates by ALD with the sequential supply of a new Al metalorganic precursor, dimethyl aluminum sec-butoxide ($C_{12}H_{30}Al_2O_2$), and water vapor (H_2O) at deposition temperatures ranging from 150 to 300 °C. The typical ALD characteristics, such as self-limited film growth behavior and linear film growth with the number of ALD reaction cycles, were observed at a deposition temperature of 250 °C. In addition, the growth rate was constant (~0.095 nm/cycle) within the ALD temperature window between 200 and 250 °C with no incubation cycles. The growth rate of the DMASBO-based ALD-Al_2O_3 process was relatively low and more controllable between 0.078 nm/cycle and 0.102 nm/cycle depending on the deposition temperature, whereas that of the TMA-based ALD-Al_2O_3 process generally showed a growth rate of ~0.125 nm/cycle, independent of the deposition temperature. The properties of the DMASBO-based ALD-Al_2O_3 thin films deposited at 250 °C were not inferior to those of the TMA-based ALD-Al_2O_3. The refractive index of the Al_2O_3 film varied from 1.45 to 1.67 depending on the deposition temperature. XPS indicated the formation of stoichiometric Al_2O_3 with no carbon impurity. The step coverage of the ALD-Al_2O_3 film was perfect, approximately 100 %, onto the overall nano-scale dual trench structure(top and bottom width: 40 and 15 nm) with an aspect ratio of ~6.3. The ALD-Al_2O_3 film has excellent thermal stability up to 1000 °C by XRD and plan-view TEM analysis. The MOS capacitor of the sputtered-Al/ALD-Al_2O_3/p-Si showed excellent performance with the ALD-Al_2O_3 film showing a dielectric constant of 8.1. The leakage current was in the order of 10^{-8} A/cm^2.

Acknowledgements

This study(2015R1A2A2A04004945) was supported by Mid-career Researcher Program through NRF grant funded by the MEST and also Human Resources Program in the Transportation Specialized Lighting Core Technology Development(No. N0001364) granted financial resource from the Ministry of Trade, Industry & Energy, Republic of Korea. The precursor used in this study was provided by Hansol Chemical Ltd.

References

1. L. Niinisto, J. Paivasaari, J. Niinisto, M. Putkonen and M. Nieminen, Phys. Status Solidi A, **201**, 1443 (2004).
2. L. G. Gosset, J.-F. Damlencourt, O. Renault, D. Rouchon, Ph. Holliger, A. Ermolieff, I. Trimaille, J.-J. Ganem, F. Martin and M.-N. Semeria, J. Non-Cryst. Solids., **303**, 17 (2002).
3. R. Katamreddy, R. Inman, G. Jursich, A. Soulet and C. Takoudis, J. Electrochem. Soc., **153**, C701 (2006).
4. D. M. Hausmann and R. G. Gordon, J. Cryst. Growth, **249**, 251 (2003).
5. A. Philip and K. Rajeev Kumar, Ph. D. Thesis, p101-128, Cochin University of Science and Technology India, (2012).
6. M. D. Groner, J. W. Elam, F. H. Fabregutte and S. M. George, Thin Solid Films., **413**, 186 (2002).
7. K. Kukli, M. Ritala and M. Leskela, J. Vac. Sci. Technol. A., **15**, 2214 (1997).
8. J. Koo, S. Kim, S. Jeon and H. Jeon, J. Korean Phys. Soc., **48**, 131 (2006).
9. M. D. Groner, J. W. Elam, F. H. Fabregutte and S. M. George, Chem. Mater., **16**, 639 (2004).
10. J. L. Hemmen, S. B. S. Heil, J. H. Klootwijk, F. Roozeboom, C. J. Hodson, M. C. M. Snaden and W. M. M. Kessels, J. Electrochem. Soc., **154**, G165 (2007).
11. F. Campabadal, J. M. Rafi, M. Zabala, O. Beldarrain, A. Faigon, H. Castan, A. Gomez, H. Garcia and S. Duenas, J. Vac. Sci. Technol. B, **29**, 01AA07 (2011).
12. E. Gerritsen, N. Emonet, C. Caillat, N. Jourdan, M. Piazza, D. Fraboulet, B. Boeck, A. Berthelot, S. Smith and P. Mazoyer, Solid State Electron., **49**, 1767 (2005).
13. L. Zhang, H. C. Jiang, C. Liu, J. W. Dong and P. Chow, J. Phys. D: Appl. Phys., **40**, 3707 (2007).
14. V. Cimalla, M. Baeumler, L. Kirste, M. Prescher, B. Christian, T. Passow, F. Benkhelifa, F. Bernhardt, G. Eichapfel, M. Himmerlich, S. Krischok and J. Pezoldt, Mater. Sci. Appl., **5**, 628 (2014).
15. R. S. Johnson, G. Lucovsky and I. Baumvol, J. Vac. Sci. Technol. A, **19**, 1353 (2001).
16. R. Katamreddy, R. Inman, G. Jursich, A. Soulet and C. Takoudis, Appl. Phys. Lett., **89**, 262906 (2006).
17. B. C. O'Regan, S. Scully, A. C. Mayer, E. Palomares and J. Durrant, J. Phys. Chem. B, **109**, 4616 (2005).

18. M. D. Groner, S. M. George, R. S. Mclean and P. F. Carcia, Appl. Phys. Lett., **88**, 051907 (2006).
19. R. S. Nowicki, J. Vac. Sci. Technol., **14**, 127 (1977).
20. C.-S. Park. J.-G. Kim and J. S. Chun, J. Vac. Sci. Technol. A, **1**, 1820 (1983).
21. J.-P. Barnes, A. K. Petford-Long, R. C. Doole, R. Serna, J. Gonzalo, A. Suarez-Garcia, C. N. Afonso and D. Hole, Nanotechnology, **13**, 465 (2002).
22. D. Hoffman and D. Leibowitz, J. Vac. Sci. Technol., **8**, 107 (1971).
23. H. Kim, H.-B.-R. Lee and W.-J Maeng, Thin Solid Films, **517**, 2563 (2009).
24. A. W. Ott, J. W. Klaus, J. M. Johnson and S. M. George, Thin Solid Films, **292**, 135 (1997).
25. M. Ritala, H. Saloniemi, M. Leskelä, T. Prohaska, G. Friedbacher and M. Grasserbauer, Thin Solid Films, **286**, 54 (1996).
26. L. Hiltunen, H. Kattelus, M. Leskelä, M. Mäkelä, L. Niinistö, E. Nykänen, P. Soininen and M. Tiitta, Mater. Chem. Phys., **28**, 379 (1991).
27. M. Ritala, M. Leskelä, J.-P. Dekker, C. Mutsaers, P. J. Soininen and J. Skarp, Chem. Vap. Deposition, **5**, 7 (1999).
28. V. E. Drozd, A. P. Baraban and I. O. Nikiforova, Appl. Surf. Sci., **82/83**, 583 (1994).
29. E. P. Gusev, M. Copel, E. Cartier, I. J. R. Baumvol, C. Krug and M. A. Gribelyuk, Appl. Phys. Lett., **76**, 176 (2000).
30. R. Matero, A. Rahtu, M. Ritala, M. Leskelä and T. Sajavaara, Thin Solid Films, **368**, 1 (2000).
31. A. W. Ott, K. C. McCarley, J. W. Klaus, J. D. Way and S. M. George, Appl. Surf. Sci., **107**, 128 (1996).
32. G. S. Higashi and C. G. Fleming, Appl. Phys. Lett., **55**, 1963 (1989).
33. S. M. George, A. W. Ott and J. W. Klaus, J. Phys. Chem., **100**, 13121 (1996).
34. T. Cheon, S.-H. Choi, S.-H. Kim and D.-H. Kang, Electrochem. Solid-State Lett., **14**, D57 (2011).
35. T. Aoyama, S. Saida, Y. Okayama, M. Fujisaki, K. Imai and T. Arikade, J. Electrochem. Soc., **143**, 977 (1996).
36. P. Ericsson, S. Bengtsson and J. Skarp, Microelectron. Eng., **36**, 91 (1997).
37. J. A. Aboaf, J. Electrochem. Soc., **114**, 948 (1967).
38. S. Yun, K. Lee, J. Skarp, H. Kim and K. Nam, J. Vac. Sci. Technol. A, **12**, 2993 (1997).
39. N. D. Hoivik, J. W. Elam, R. J. Linderman, V. M. Bright, S. M. George and Y. C. Lee, Sens. Actuators A Phys., **103**, 100 (2003).
40. O. M. E. Ylivaara, X. Liu, L. Kilpi, J. Lyytinen, D. Schneider, M. Laitinen, J. Julin, S. Ali, S. Sintonen, M. Berdova, E. Haimi, T. Sajavaara, H. Ronkainen, H. Lipsanen, J. Kosoinen, S.-P. Hannula and R. L. Puurunen, Thin Solid Films, **552**, 124 (2014).
41. S. Kim, S. Lee, C, Hwang, Y. Min, J. Won and J. Jeong, J. Electrochem. Soc., **153**, F69 (2006).
42. S. K. Pradhan, P. J. Reucroft and Y. Ko, Surf. Coat. Technol., **176**, 382 (2004).
43. P. katiyar, C. Jin and R. J. Narayan, Acta Mater., **53**, 2617 (2005).
44. S. Jakschik, U. Schroeder, T. Hecht, M. Gutsche, H. Seidl and J. W. Bartha, Thin Solid Films, **425**, 216 (2003).